The wave equation for pressure given above has a direct analog in electromagnetic theory, where the scalar potential (for the electric field) replaces the pressure, and the charge density constitutes the source rather than the heat deposition rate. Given this simple analogy and the comprehensive investigation of Maxwell's equations that has taken place over the last century, it is natural to ask why electromagnetic solutions analogous to Eqs. 2, 4, and 5 have not appeared. The answer to this question lies in an important distinction between the kinds of sources that are possible according to acoustic and electromagnetic theory: the photoacoustic wave forms described here arise from monopole radiation resulting from a uniform expansion of the body that is naturally produced by the absorption of radiation—the analogous rapid switching on of a macroscopic quantity of electrical charge of a single polarity that would constitute a monopole source of electromagnetic radiation is not possible under the restriction of charge conservation.

REFERENCES AND NOTES

1. P. Hess, Ed. *Photoacoustic, Photothermal and Photochemical Processes in Gasses* (Springer-Verlag, Heidelberg, 1989); M. W. Sigrist, *J. Appl. Phys.* **60**, R83 (1986); A. C. Tam, *Rev. Mod. Phys.* **58**, 381 (1986); E. Luscher, H. J. Coufal, P. Korpium, R. Tilgner, Eds., *Photoacoustic Effect, Principles and Applications*, (Viewig, Braunschweig, West Germany, 1984); A. C. Tam, in *Ultrasensitive Laser Spectroscopy*, D. S. Kilger, Ed. (Academic Press, New York, 1983), pp. 1–108.
2. The photoacoustic effect in a homogeneous medium has been discussed by a number of investigators, including: H. C. Hu, *J. Acoust. Soc. Am.* **48**, 2245 (1969); J. M. Heritier, *Opt. Commun.* **44**, 267 (1983); H. M. Lai and K. Young, *J. Acoust. Soc. Am.* **72**, 2000 (1982); L. M. Lyamshev, *Sov. Phys. Usp.* **24**, 977 (1981); L. M. Lyamshev and L. V. Sedov, *Sov. Phys. Acoust.* **27**, 4 (1981); N. W. Sigrist and F. K. Kneubuhl, *J. Acoust. Soc. Am.* **64**, 1652 (1978). Some work has been published where acoustic waves are generated by thermal conduction. See A. Yoshinaga, Y. Hsieh, T. Sawada, Y. Gohshi, *Anal. Sci.* **5**, 147 (1989); T. Kitamori and M. Fujii, *J. Appl. Phys.* **58**, 1456 (1985); C. W. Bruce and R. G. Pinnick, *Appl. Opt.* **16**, 1762 (1977); Z. Yasa, N. Amer, H. Rosen, A. D. Hansen, T. Novakov, *ibid.* **18**, 2428 (1979).
3. The wave equation for pressure can be used when heat conduction can be neglected on the time scale for sound wave generation.
4. P. J. Westervelt and R. S. Larson, *J. Acoust. Soc. Am.* **54**, 121 (1973); S. Temkin, *Elements of Acoustics* (Wiley, New York, 1981).
5. G. J. Diebold and P. J. Westervelt, *J. Acoust. Soc. Am.* **84**, 2245 (1988).
6. Specifically, the retarded time is defined as $\hat{\tau} = (c_s/a)[t - (r - a)/c_f]$ for a sphere, where t is the time after firing of the laser, a is the radius of the sphere, and c_f is the sound speed in the fluid. For a cylinder $\hat{\tau}$ and κ are given by the same expression, but $\hat{r}$ is expressed in polar coordinates, c_s refers to the sound speed in the cylinder, a is the radius of the cylinder, and $t = c_s t/a$. For a fluid layer, $\hat{\tau} = (2c_f/a)[t - (z - a/2)/c_f]$, where a now refers to the thickness of the layer and c_f is the sound speed in the slab. The parameter κ in these three geometries refers to quantities in the radiation-absorbing medium.
7. The rise times and other high-frequency features of the experimental wave forms are intrinsically limited by the finite duration of the laser pulse (approximately 10 ns here), and by viscous effects in the fluid that have not been taken into account in the theory. In the case of spherical and cylindrical waves, integration of the wave forms over the face of the detector also causes an apparent decrease in the recorded rise time. These effects are clearly evident in the cylindrical wave forms. The dimensions of the spheres and cylinders are determined by measuring the shadows they cast on a screen. For features δt of the wave forms that correspond to transit times across the particles, agreement with theory to within 20% is obtained in all the experiments.
8. H. Coufal, in *Photoacoustic and Photothermal Phenomena*, P. Hess and J. Pelzl, Eds. (Springer-Verlag, Heidelberg, 1988), pp. 464–469.
9. L. D. Landau and E. M. Lifshitz, *Fluid Mechanics* (Pergamon, New York, 1987), p. 273.
10. R. B. Lindsay, *Mechanical Radiation* (McGraw-Hill, New York, 1960).
11. Glass supports a shear wave and cannot be considered as a fluid. However, for a plane wave directed at perpendicular incidence to an infinite solid surface, no transverse wave is generated and the analysis given here remains valid.

12. We are grateful to P. J. Westervelt for his helpful contributions and discussion and to J. Taylor and R. Boyles for their skillful construction of the experimental apparatus. Supported under grant ER13235 from the U.S. Department of Energy Office of Basic Energy Sciences.

10 April 1990; accepted 29 June 1990

A Bangiophyte Red Alga from the Proterozoic of Arctic Canada

NICHOLAS J. BUTTERFIELD, ANDREW H. KNOLL, KEENE SWETT

Silicified peritidal carbonate rocks of the 1250- to 750-million-year-old Hunting Formation, Somerset Island, arctic Canada, contain fossils of well-preserved bangiophyte red algae. Morphological details, especially the presence of multiseriate filaments composed of radially arranged wedge-shaped cells derived by longitudinal divisions from disc-shaped cells in uniseriate filaments, indicate that the fossils are related to extant species in the genus *Bangia*. Such taxonomic resolution distinguishes these fossils from other pre-Edicaran eukaryotes and contributes to growing evidence that multicellular algae diversified well before the Ediacaran radiation of large animals.

MULTICELLULAR ORGANISMS characterized by cellular integration and differentiation occur in all four eukaryotic kingdoms, including at least eight separate phyla in the Protista (*1*). Most of these experiments in complex multicellularity must have made their first appearance well before the Edicaran radiation of large animals (600 million years ago, Ma), but fossil evidence is limited and in many cases equivocal. Interpretational problems result from the lack of preserved cellular structure in many fossils, the nondiagnostic nature of such structures as may be preserved, and the absence of biochemical and ultrastructural information. In this report, we describe well-preserved fossils in 1250- to 750-million-year-old rocks from arctic Canada in which the habit and patterns of cell division are sufficiently distinctive to permit their assignment to the bangiophyte red algae.

The fossiliferous rocks were collected on Somerset Island, a narrowly separated extension of the Boothia Peninsula in the southeastern part of the Canadian arctic archipelago (District of Franklin, Northwest Territories) (Fig. 1). In the Aston Bay area on its northwest coast, little altered middle to upper Proterozoic sedimentary rocks sit on crystalline basement of the Canadian Shield (*2*). The sedimentary sequence comprises two unconformity-bounded units. The lower unit, the Aston Formation, consists largely of quartz arenite, whereas the overlying Hunting Formation is dominated by intertidal to supratidal carbonate rocks. The fossiliferous horizons are thin (1 cm thick) chert layers in stratiform laminated shallow-subtidal to intertidal carbonate rocks of the Hunting Formation, approximately 150 m above the Aston-Hunting contact.

Hunting deposition is only broadly constrained in time, bracketed by two generations of mafic dikes (*2*) that are dated elsewhere at 1267 ± 2 Ma (*3*) and 723 ± 3 Ma (*4*). Constituent stromatolites (stratiform to simple *Baicalia*-type columns) and associated microfossils (dense filamentous mats, spheroids, and the stalk-forming cyanobacterium *Polybessurus*) are useful as paleoenvironmental indicators but cannot provide finer time resolution. On the other hand, several analyses of Hunting carbonate rocks indicate that they have $\delta^{13}C$ values between +2.5 and +3.8 per mil (*5*), values lighter than those typical of 700- to 800-million-year-old carbonate rocks in the Canadian arctic and elsewhere (*5, 6*). The Hunting isotopic signature more closely approximates that of unweathered dolomite from the 1100- to

N. J. Butterfield and A. H. Knoll, Botanical Museum, Harvard University, Cambridge, MA 02138.
K. Swett, Department of Geology, University of Iowa, Iowa City, IA 52242.

1200-million-year-old Mescal Limestone, Arizona (*7*), and 1150- to 1300-million-year-old marble of the Upper Marble unit, Grenville Series, New York (*8*). Thus, the carbon isotopic evidence, although not definitive, suggests that Hunting sedimentation might have occurred closer to the older rather than the younger dike-defined chronological boundary.

The fossils are moderately to extraordinarily well preserved, having been permineralized by very early diagenetic chert. Petrographic thin sections cut perpendicular to bedding have so far exposed over 500 fossil filaments. In their most simple (and most common) state, the fossils consist of stacked disc-shaped cells enclosed in a relatively transparent enveloping sheath and form unbranched uniseriate filaments 15 to 45 μm in diameter and up to 2 mm long (Fig. 2). Almost all of the fossils are oriented vertically and they commonly occur in groups attached to locally stabilized surfaces (Fig. 2A); the basal ends of the filaments are elaborated into multicellular structures that appear to serve as attachment rhizoids (Fig. 3). Larger diameter specimens (>45 μm across) of these same populations are generally multiseriate with a number of cells occupying any given level along the filament (Figs. 2B and 4B). Transverse cross sections of these more complex forms (Fig. 4C) reveal that the component cells are wedge-shaped and arranged axially around a central core. The specimen in Fig. 4C preserves three of what were originally eight such cells, and in different focal planes of the same specimen, four adjacent layers show a similar pattern of cell division. Other filaments have a fourfold radial cleavage (b in Fig. 2B).

In most details of their morphology, and particularly in their distinctive patterns of cell division, these fossil filaments compare closely to the gametophytic (1N) generation of species belonging to the modern red algal genus *Bangia* (Bangiaceae, Bangiales, Bangiophyceae, Rhodophyta). *Bangia* is a cosmopolitan seaweed that today ranges from boreal to subtropical oceans and from marine waters to freshwater lakes and streams (*9–13*). It tolerates extended emersion and desiccation and is usually found in the upper intertidal zone of marine coastlines and at or above the waterline in fresh water; it commonly occurs with filamentous cyanobacteria above the zone occupied by green algae (*9, 11*).

In its most simple form, gametophytic *Bangia* is characterized by unbranched uniseriate filaments composed of stacked, disc-shaped cells. The polysaccharide cell walls are distinctly biphasic with an inner wall defining individual cells and an outer wall enveloping the whole organism (*14*) (Fig. 4D). In more mature, multiseriate forms this 'outer' wall also occupies the central core of the filament (Fig. 4F); a sub-micron thick "cuticle" gives the filament a sharply delineated boundary layer (*14*). Unlike the apical cell division typical of florideophyte red algae, vegetative growth in bangiophytes generally occurs by transverse intercalary cell division (*12, 13, 15*); consequently, *Bangia* filaments often show a hierarchical packaging of successive cell generations (Fig. 4D). In the fossil filaments both a differentiated inner and outer cell wall and a pattern of transverse intercalary cell divisions are clearly evident (Figs. 2B and 4A).

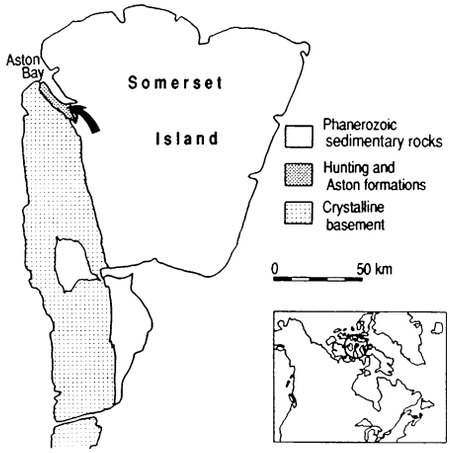

Fig. 1. Schematic geological map of Somerset Island showing the location of fossiliferous Hunting Formation strata.

Mature filaments of *Bangia* generally become multiseriate through longitudinal intercalary division (*12, 14*) (Fig. 4E). They do not, however, become simple constructions of randomly arranged, equidimensional cells. Not only is the position of each parent cell broadly retained in the multiseriate filament, but initial cleavage of the disc-shaped cells is also radially oriented. This orientation yields a distinctive pattern of wedge-shaped cells arranged axially around a central core (*12, 14*) and is particularly apparent in transverse cross sections of mature *Bangia* filaments (Fig. 4F). Because many of the gross morphological characteristics of sub–tissue grade organisms are convergent or ecophenotypic (*9, 10, 13, 16*), such underlying cellular patterns are likely to be of considerable phylogenetic significance. Along with its other cellular and extracellular details, the radial pattern of cells in the fossil material strongly supports its assignment to the bangiophyte red algae, possibly to the level of family (Bangiaceae).

The fossils are not identical to extant species of *Bangia*. The modern alga varies widely in filament width but averages 100 μm diameter (*10*). The Proterozoic filaments fall in the size range of modern *Bangia* but are generally smaller, having a mean diameter of 26 μm (n = 519; SD = 7.4 μm) and a minor mode of 53 μm in the case of multiseriate forms (n = 13; SD = 9.1 μm). Maximum measured diameter in our samples is 72 μm. The fossils also differ in possessing multicellular rhizoids or holdfast structures (Fig. 3), whereas *Bangia* has long, nonseptate rhizoids descending from a number of basal vegetative cells (*12*). Multicellular rhizoids are nevertheless common in the red algae, and holdfasts essentially identical to those of the fossils are found in the filamentous bangiophytes *Erythrotrichia* (Erythropeltidaceae) and *Porphyra* (Bangiaceae) (*12, 13*).

Are there other possible interpretations of these fossils? Stigonematacean cyanobacteria often form a comparably thick external sheath and are commonly multiseriate. However, these prokaryotes are also characterized by true branching and several types of differentiated cells (for example, heterocysts and akinetes), which are not observed in the fossils. More importantly, the multiseriate thallus of stigonemataceans appears to be a relatively loose knit association of cells and filaments lacking any particular

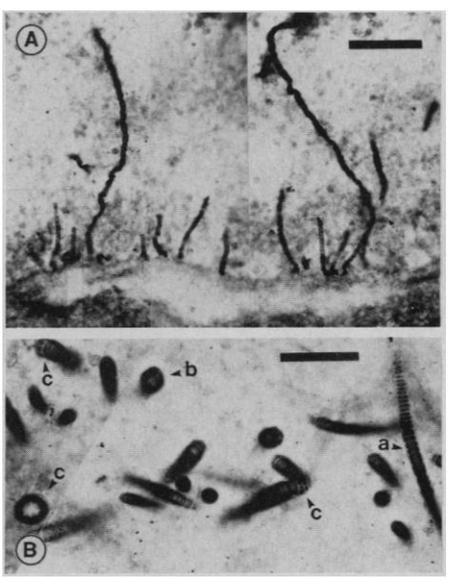

Fig. 2. Populations of fossil bangiophyte filaments in petrographic thin sections of Hunting Formation chert cut perpendicular to bedding. (**A**) Low magnification photomicrograph illustrating the vertical orientation and substrate attachment of the fossils; scale bar equals 0.25 mm. (**B**) Fossil filaments showing a number of morphological features characteristic of bangiophytes: a, uniseriate filament consisting of ensheathed paired cells; b, transverse cross section of a filament showing fourfold radial cleavage; c, transverse, oblique, and longitudinal cross sections of multiseriate filaments with approximate eightfold radial cleavage; scale bar equals 0.15 mm.

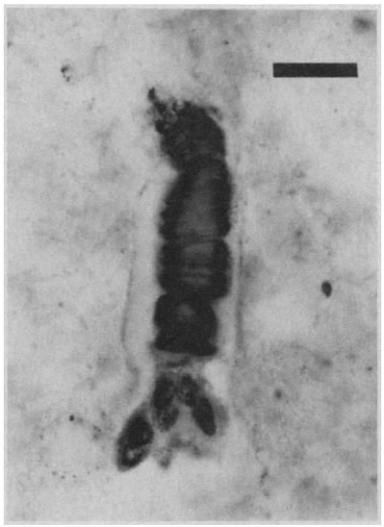

Fig. 3. Basal portion of a fossil filament showing the multicellular rhizoid structure; scale bar equals 30 μm.

geometrical or developmental regularity (*17*); the distinctive pattern of radial cell division characteristic of both *Bangia* and the fossil material is unknown in any cyanobacterium (*18*). Other extant eukaryotes, such as species of the green algal family Schizomeridaceae, likewise form uniseriate and multiseriate filaments (*13*), but these also lack radially oriented cells.

These fossils are neither the only nor the oldest Proterozoic metaphytes. Undoubted multicellular algae are known from several late Riphean (900 to 700 Ma) shale biotas and include coenobial colonies (*19*) and branching filamentous forms, both septate (*20*) and coenocytic (*21*). Macroscopic tawuiids and lonfengshaniids (1100 to 700 Ma) have a worldwide distribution and represent at least probable metaphytes (*22*), as do filamentous macrofossils in 1400-million-year-old deposits from Montana and China (*23*). Problematic bedding plane markings in middle Proterozoic sandstones of Western Australia may be imprints of a relatively large filamentous seaweed (*24*). In latest Proterozoic rocks a calcareous, encrusting phylloid alga (*25*) and a variety of structured multicellular fossils (*26*) have been documented, and filamentous organic-walled vendotaenids are generally, although not universally (*27*), thought to be of algal origin (*28*). None of these fossils, however, can be placed confidently into any extant higher-order taxon. The same can be said for most of the organic-walled fossil algae of Phanerozoic age (*16*). In contrast, the clearly interpretable morphology of the Somerset Island fossils provides a detailed datum point for the reconstruction of early red algal and protistan phylogeny.

The two classes of the Rhodophyta, Bangiophyceae and Florideophyceae, are distinguished on the basis of thallus form, growth habit, and various intracellular characteristics (*12, 13, 15*). They appear to be linked phylogenetically by the microscopic chonchocelis phase (2N sporophyte) observed in some species of *Bangia* and *Porphyra* (Bangiaceae); the conchocelis exhibits a number of otherwise florideophyte characteristics (*15*). The Bangiophyceae are generally considered to be less advanced than, although not necessarily ancestral to, the Florideophyceae (*13*). As gametophytic bangiophytes, the Hunting Formation fossils predate the earliest record of probable florideophytes (*16*) by at least 200 million years and thus provide at least circumstantial support for a bangiophyte to florideophyte phylogenesis. Whether the bangiophyte life cycle included an alternation of generations by Hunting time is speculative at this point as we have found no evidence of a chonchocelis phase in our samples. The oldest reported chonchocelis comes from Silurian rocks in Poland (*29*).

Molecular data from both small subunit (*30*) and large subunit (*31*) ribosomal RNA suggest that the three principal clades containing multicellular algae (Rhodophyta, Chlorophyta, Phaeophyta) diverged during a brief but marked radiation relatively late in eukaryotic history. This interpretation is broadly supported by the moderate diversity of mid to late Proterozoic fossil metaphytes. Multicellularity, however, is almost certainly a derived condition, and Tappan's (*32*) interpretation of the 2000-million-year-old Gunflint microfossil *Eosphaera* as a *Porphyridium*-like rhodophyte, although controversial, underscores the probability that unicellular red, green, and chromophyte algae antedated their multicellular descendants by a significant interval. Although the timing of early algal diversification remains incompletely known, the Hunting Formation fossils contribute to a growing paleontological record which indicates that several and perhaps all major groups of multicellular algae were well established long before the Ediacaran and Cambrian radiations.

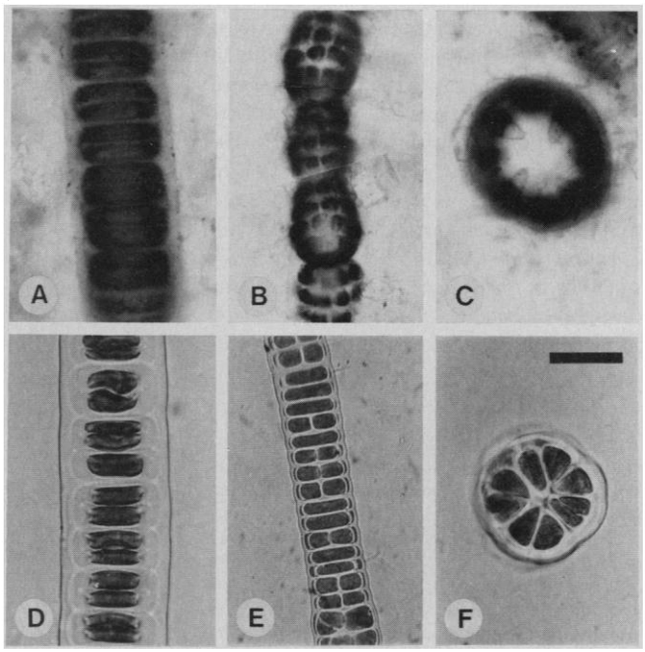

Fig. 4. Comparison of fossil filaments (A to C) with modern *Bangia atropurpurea* (collected at Marblehead, Massachusetts, January, 1990) (D to F). (**A**) Uniseriate filament showing the hierarchical packaging of cells into pairs and quartets indicative of intercalary cell division; all cells are enclosed in a sharply delineated outer wall. (**B**) Multiseriate filament with a number of constrictions (similar constrictions are also found in modern *Bangia*). (**C**) Transverse cross section of a multiseriate filament with an eight-fold radial cleavage. Three complete, wedge-shaped cells are visible, and the bases of an additional five cells can be discerned. (**D**) Longitudinal cross section of a uniseriate *Bangia* filament showing the inner and outer cell walls and the hierarchical packaging of cell pairs. (**E**) Longitudinal cross section of multiseriate *Bangia*. (**F**) Transverse cross section of a multiseriate *Bangia* filament showing an approximate eight-fold radial cleavage and a central core of "outer wall." Scale bar [shown in (F)] equals 20 μm for (A); 50 μm for (B); 30 μm for (C); 35 μm for (D); 80 μm for (E); and 50 μm for (F).

REFERENCES AND NOTES

1. L. W. Buss, *The Evolution of Individuality* (Princeton Univ. Press, Princeton, 1987).
2. W. D. Stewart, *Geol. Surv. Can. Pap. 83-26* (1987).
3. A. N. LeCheminant and L. M. Heaman, *Earth Planet. Sci. Lett.* **96**, 38 (1989).
4. L. M. Heaman and R. H. Rainbird, *Geol. Assoc. Can. Prog. Abstr.* **15**, A55 (1990).
5. N. J. Butterfield, A. H. Knoll, J. M. Hayes, unpublished data; $\delta^{13}C$ is defined as

$$\delta^{13}C = \left[\frac{^{13}C/^{12}C_{sample}}{^{13}C/^{12}C_{standard}} - 1\right] \times 10^3$$

and reported in parts per mil relative to the Pee Dee Belemnite (PDB) standard.
6. A. H. Knoll, J. M. Hayes, A. J. Kaufman, K. Swett, I. B. Lambert, *Nature* **321**, 832 (1986).
7. M. A. Beeunas and L. P. Knauth, *Geol. Soc. Am. Bull.* **96**, 737 (1985).
8. J. F. Whelan, R. O. Rye, W. deLorraine, H. Ohmoto, *Am. J. Sci.* **290**, 396 (1990).
9. R. G. Sheath and K. M. Cole, *J. Phycol.* **16**, 412 (1980).
10. ———, *Phycologia* **23**, 383 (1984).
11. R. G. Sheath, K. L. VanAlstyne, K. M. Cole, *J. Phycol.* **21**, 297 (1985).
12. D. J. Garbary, G. I. Hansen, R. F. Scagel, *Syesis* **13**,

137 (1980).
13. H. C. Bold and M. J. Wynne, *Introduction to the Algae* (Prentice-Hall, Englewood Cliffs, NJ, ed. 2, 1986); F. E. Fritsch, *The Structure and Reproduction of the Algae* (Cambridge Univ. Press, Cambridge, 1965).
14. K. M. Cole, C. M. Park, P. E. Reid, R. G. Sheath, *J. Phycol.* **21**, 585 (1985).
15. K. Cole and E. Conway, *Phycologia* **14**, 239 (1975).
16. C. D. Walcott, *Smithsonian Misc. Coll.* **67**, 217 (1919); W. L. Fry, *Rev. Palaeobot. Palynol.* **39**, 313 (1983).
17. T. C. Martin and J. T. Wyatt, *J. Phycol.* **10**, 57 (1974).
18. S. Golubic, personal communication.
19. N. J. Butterfield and A. H. Knoll, *Geol. Soc. Am. Abstr. Prog.* **21**, A146 (1989).
20. N. J. Butterfield, A. H. Knoll, K. Swett, *Nature* **334**, 424 (1988).
21. T. N. German, *Paleontol. J.* **1981**, no. 2, 100 (1981).
22. H. J. Hofmann, in *Paleoalgology: Contemporary Research and Applications*, D. F. Toomey and M. H. Nitecki, Eds. (Springer-Verlag, Berlin, 1985), pp. 20–33.
23. M. R. Walter, J. H. Oehler, D. Z. Oehler, *J. Paleontol.* **50**, 872 (1976); Du Rulin, Tian Lifu, Li Hanbang, *Acta Geol. Sinica* **1986**, no. 2, 115 (1986).
24. K. Grey and I. R. Williams, *Precambr. Res.* **46**, 307 (1990).
25. S. W. F. Grant and A. H. Knoll, *Geol. Soc. Am. Abstr. Prog.* **19**, 681 (1987).
26. Zhang Y., *Lethaia* **22**, 113 (1989).
27. G. Vidal, *ibid.*, p. 375.
28. M. B. Gnilovskaya, Ed., *Vendotaenids of the East European Platform* (Nauka, Leningrad, 1988).
29. S. Campbell, *J. Phycol.* **19**, 25 (1980).
30. D. Bhattacharya, H. J. Elwood, L. J. Goff, M. L. Sogin, *ibid.* **26**, 181 (1987).
31. R. Perasso, A. Baroin, L. H. Qu, J. P. Bachellerie, A. Adoutte, *Nature* **339**, 142 (1990).
32. H. Tappan, *Geol. Soc. Am. Bull.* **87**, 633 (1976).
33. We thank the National Geographic Society, the National Science Foundation, and the Department of Energy for supporting field and laboratory work, and the Canadian Polar Continental Shelf Project for logistic support in the field. S. Golubic first pointed out the bangiophyte habit of the fossil material and D. Bhattacharya provided useful phylogenetic information; the comments of an anonymous reviewer concerning modern *Bangia* biology were particularly instructive. N.J.B. is supported by a Natural Sciences and Engineering Research Council of Canada post-graduate scholarship.

16 April 1990; accepted 25 July 1990

Not So Hot "Hot Spots" in the Oceanic Mantle

ENRICO BONATTI

Excess volcanism and crustal swelling associated with hot spots are generally attributed to thermal plumes upwelling from the mantle. This concept has been tested in the portion of the Mid-Atlantic Ridge between 34° and 45° (Azores hot spot). Peridotite and basalt data indicate that the upper mantle in the hot spot has undergone a high degree of melting relative to the mantle elsewhere in the North Atlantic. However, application of various geothermometers suggests that the temperature of equilibration of peridotites in the mantle was lower, or at least not higher, in the hot spot than elsewhere. The presence of H_2O-rich metasomatized mantle domains, inferred from peridotite and basalt data, would lower the melting temperature of the hot spot mantle and thereby reconcile its high degree of melting with the lack of a mantle temperature anomaly. Thus, some so-called hot spots might be melting anomalies unrelated to abnormally high mantle temperature or thermal plumes.

THE CONCEPT OF HOT SPOTS HAS played an important role in the theory of plate tectonics (*1–3*). Oceanic hot spots are areas of thicker than normal crust and excess volcanism and are commonly marked by islands. They are generally attributed to anomalously high temperatures of upwelling mantle plumes, which result in overabundant production of melt and in crustal swelling (*1–4*). In this report I discuss data from one such inferred hot spot, the Azores hot spot complex (AHS), located between 34° and 45°N in the Mid-Atlantic Ridge (MAR). These data imply that this so-called hot spot may not be caused by anomalously high upper-mantle temperatures, but rather by a mantle with a composition different from that underlying normal segments of the Mid-Atlantic Ridge.

The geochemical nature of the oceanic upper mantle has been inferred from studies of the melts extracted from it (oceanic basalts) or of the solid residue left behind in the mantle after melt extraction (oceanic peridotites). The reconstructed primary mineralogy of oceanic peridotites [olivine + orthopyroxene (opx) ± clinopyroxene (cpx) + spinel] suggests that they equilibrated in the spinel peridotite facies [pressure >8 to 9 kbar at 1000° to 1300°C (*5*)]. I compare the chemistry of these mantle-equilibrated relic phases in samples of peridotite bodies emplaced in young (<35 million years old) North Atlantic crust (Fig. 1) and representing the uppermost sub-Atlantic mantle [see (*6–8*) for methods and raw data].

Regional, long-wavelength (~1000 km) variations of peridotite modal and mineral composition (Fig. 2), detected along the MAR (*6, 9*), must reflect fundamental regional differences in upper mantle composition, thermal structure, or both (*10*). The chemistry of the primary minerals, namely their content of Mg, Cr, and other refractory elements versus that of Al, Fe, and other incompatible elements (*10–12*), suggest that greater amounts of melt [up to >20% melting relative to a pyrolite-like source (*6*)] have been extracted from the mantle rocks in the AHS region than elsewhere in the MAR, where the degree of melting can be as low as 8% (*6*). These regional variations along the MAR are associated with variations of geophysical parameters (Fig. 2) such as zero-age sea-floor depth (*13*) and geoid residual anomaly (*14*), and basalt properties such as Na_2O content (*15*) and La/Sm ratio (*16*). Basalt Na_2O content has been related to the degree of partial melting undergone by the source material in the mantle (*15*). It is inversely correlated with the 100Cr/(Cr + Al) ratio of spinels in peridotite. Along with other mineral chemistry relations (*6*), it provides independent support for high degree of melting of the AHS mantle.

This high degree of melting could reflect higher upper-mantle temperatures in the AHS than elsewhere along the MAR, consistent with the notion that the anomalous region is a hot spot (*15, 16*). If temperature differences in the upper mantle were the sole cause of the different degrees of melting, estimated differences in mantle temperature between mid-ocean ridge segments with highest and lowest extent of melting should be ~250° to ~300°C at equivalent depths in the melting region (*15*). If we consider only the North Atlantic part of the ridge, these differences are reduced somewhat. The temperature differences would be smaller at shallower depth in the mantle where final subsolidus equilibration of the peridotite occurs, but should still exceed 100°C.

In order to test the assumption that mantle temperature is the cause of differences in the degree of melting along the MAR, I have calculated peridotite equilibration temperatures using the Wells' (*17*) and Lindsley's (*18, 19*) geothermometers. Both are based on the temperature dependence of reactions between coexisting opx and cpx (*20, 21*). Among the various proposed peridotite geothermometers, these appear to be the most reliable, particularly for peridotites equilibrated in the spinel lherzolite stability field (*22*). However, because of the limitations of these and other peridotite geothermometers, I regard the estimated temperatures (Fig. 2) as expressing relative trends rather than absolute values (*23*). The calculated temperatures are generally consistent within each geotectonic area (*24–26*).

Lamont-Doherty Geological Observatory of Columbia University, Palisades, New York 10964.